

1 Dear Editor:

2 In order to avoid a lengthy and repetitive response letter, please find our point-by-point responses in the  
3 authors' comments we uploaded to BGD discussion forum.

4 We have, however, included a manuscript with changes tracked to show all relevant changes we made to  
5 improve the manuscript.

6 We thank you for your time and look forward to hear from you.

7 Yuanyuan on behalf of all co-authors

8

9           **Using atmospheric observations to evaluate the**  
10           **spatiotemporal variability of CO<sub>2</sub> fluxes simulated by**  
11           **terrestrial biospheric models**

12           Yuanyuan Fang<sup>1</sup>, Anna M. Michalak<sup>1</sup>, Yoichi P. Shiga<sup>1,2</sup>, Vineet Yadav<sup>1</sup>

13           <sup>1</sup> Department of Global Ecology, Carnegie Institution for Science, Stanford, CA, USA

14           <sup>2</sup> Department of Civil and Environmental Engineering, Stanford University, Stanford, CA, USA

15  
16           Correspondence to: Yuanyuan Fang (yyfang@stanford.edu)

## Abstract

17  
18 Terrestrial biospheric models (TBMs) are used to extrapolate local observations and process-  
19 level understanding of land-atmosphere carbon exchange to larger regions, and serve as a  
20 predictive tool for examining carbon-climate interactions. Understanding the performance of  
21 TBMs is thus crucial to the carbon cycle and climate science. In this study, we ~~propose a~~  
22 ~~statistical model selection~~ present and assess an approach for evaluating the spatiotemporal  
23 patterns, rather than aggregated magnitudes, of net ecosystem exchange (NEE) simulated by  
24 TBMs using atmospheric CO<sub>2</sub> measurements. ~~We~~ The approach is based on statistical model  
25 selection implemented within a high-resolution atmospheric inverse model. Using synthetic data  
26 experiments, we find that current atmospheric observations are sensitive to the underlying  
27 spatiotemporal flux variability at sub-biome scales for a large portion of ~~the~~ North American  
28 ~~continent~~ America, and that atmospheric observations can therefore be used to evaluate simulated  
29 spatiotemporal flux patterns, ~~rather than focusing solely on flux magnitudes at aggregated scales.~~  
30 ~~Results show that the proposed approach can be used to assess whether a TBM represents a~~  
31 ~~substantial portion of the underlying flux variability~~ as well as to differentiate among multiple  
32 competing TBMs. ~~When applying the proposed approach to~~ Experiments using real atmospheric  
33 observations and four prototypical TBMs, ~~we find~~ further confirm the applicability of the  
34 method, and demonstrate that the performance of TBMs in simulating the spatiotemporal  
35 patterns of NEE varies substantially across seasons, with best performance during the growing  
36 season and more limited skill during transition seasons. This seasonal difference in the result is  
37 consistent with previous work showing that the ability of TBMs to ~~represent the spatiotemporal~~  
38 ~~flux variability may reflect the models' capability to represent the~~ model flux magnitudes is also  
39 ~~seasonally-varying influence of environmental drivers of flux. While none of the TBMs~~  
40 ~~consistently outperforms the others, differences among the examined models are at least partially~~

41 | ~~attributable to their internal structures dependent.~~ Overall, the proposed approach provides a  
42 | new avenue for evaluating TBM performance based on sub-biome scale flux patterns, presenting  
43 | an opportunity for assessing and informing model development using atmospheric observations.

44

45 **1 Introduction**

46 A key question in ~~the~~ carbon cycle science is how terrestrial carbon sinks will evolve within the  
47 context of a rapidly changing climate. Such projections of future carbon-climate interactions  
48 largely depend on the accuracy of current terrestrial biospheric models (TBMs), the main tool  
49 used to simulate the processes controlling the biospheric carbon cycle. Thus, understanding and  
50 evaluating the performance of current TBMs is an essential step toward improving the state of  
51 carbon cycle research.

52 TBM predictions of carbon flux can be directly evaluated against eddy covariance tower  
53 measurements at various time scales ranging from hourly to interannual (~~Baker et al., 2003;~~  
54 ~~Balzarolo et al., 2013; Keenan et al., 2012; Raczka et al., 2013; Richardson et al., 2012; Sasai et~~  
55 ~~al., 2005; Schaefer et al., 2012; Schwalm et al., 2010)~~(Baker et al., 2003; Balzarolo et al., 2014;  
56 ~~Keenan et al., 2012; Raczka et al., 2013; Richardson et al., 2012; Sasai et al., 2005; Schaefer et~~  
57 ~~al., 2012; Schwalm et al., 2010),~~ but the information provided by flux towers is only  
58 representative of small spatial scales (~1km<sup>2</sup>) relative to the scales of interest for global  
59 ~~simulationsanalyses~~. On the other end of the spectrum, TBM predictions aggregated to large  
60 spatial and/or temporal scales (*e.g.*, continental/monthly to global/annual) are routinely  
61 intercompared with flux estimates obtained from inverse-modeling ~~estimates~~-based on observed  
62 atmospheric CO<sub>2</sub> mixing ratios (~~Canadell et al., 2011; Gourdji et al., 2012; Hayes et al., 2012;~~  
63 ~~McGuire et al., 2012; Turner et al., 2011)~~(Canadell et al., 2011; Gourdji et al., 2012; Hayes et al.,  
64 ~~2012; McGuire et al., 2012; Turner et al., 2011),~~ but such large-scale comparisons make it  
65 difficult to provide directly usable information regarding the processes driving carbon exchange.  
66 In addition, differences among TBMs exist across a full range of spatiotemporal scales, including  
67 inter-annual variability, the timing of phenology, and the spatiotemporal distribution of

Formatted: Font color: Text 1

68 biospheric carbon fluxes within regions (~~Gourdji et al., 2012; Huntzinger et al., 2012; Keenan et~~  
69 ~~al., 2012; Raczka et al., 2013; Richardson et al., 2012; Schaefer et al., 2012; Schwalm et al.,~~  
70 ~~2010~~)(Gourdji et al., 2012; Huntzinger et al., 2012; Keenan et al., 2012; Raczka et al., 2013;  
71 Richardson et al., 2012; Schaefer et al., 2012; Schwalm et al., 2010). These differences reflect  
72 the fact that processes controlling carbon-climate feedbacks are manifested differently across  
73 TBMs.

74 Assessing the spatial and/or temporal variability of carbon fluxes as a method for evaluating  
75 TBMs, therefore, offers the potential to examine the environmental processes driving carbon  
76 exchange, and hence provides ~~a novel~~ an alternative path forward in the assessment of TBM  
77 predictions. For example, evaluating the timing of modeled phenology can highlight issues  
78 associated with a model's representation of Light Use Efficiency (LUE), temperature response,  
79 and GPP response under various conditions (~~Richardson et al., 2012; Schwalm et al.,~~  
80 ~~2010~~)(Richardson et al., 2012; Schwalm et al., 2010). Examining the interannual variability of  
81 TBM output can identify problems with the representation of interannual variability in spring  
82 phenology, soil thaw, snowpack melt and lagged response to extreme climatic events (~~Keenan et~~  
83 ~~al., 2012~~)(Keenan et al., 2012).

84 The majority of previous studies examining carbon flux variability are still based on spatially  
85 and/or temporally aggregated carbon fluxes, however. An evaluation of flux variability, or flux  
86 patterns, at the fine native spatiotemporal scales of TBM simulations would make it possible to  
87 more directly target the fine-scale spatiotemporal patterns of carbon fluxes that have been shown  
88 to directly relate to environmental/climatic factors, such as precipitation, radiation and nighttime  
89 temperature (~~Beer et al., 2010; Mueller et al., 2010; Yadav et al., 2010~~)(Beer et al., 2010;

90 Mueller et al., 2010; Yadav et al., 2010). Such evaluations could therefore inform model  
91 improvements at the process level.

92 Observations of atmospheric CO<sub>2</sub> can potentially be used to assess such fine-scale  
93 spatiotemporal flux patterns. Variations On one hand, atmospheric CO<sub>2</sub> observations are sensitive  
94 to fine-scale NEE spatial and temporal variability (Huntzinger et al., 2011). On the other hand,  
95 variations in atmospheric CO<sub>2</sub> measurements are routinely used in inverse modeling frameworks  
96 to infer upwind sources and sinks of CO<sub>2</sub>, and recent studies suggest that atmospheric  
97 observations contain information about flux patterns at spatial and temporal resolutions  
98 comparable to those of TBMs run for regional to continental to global domains (Broquet et al.,  
99 2013; Gökede et al., 2010; Gourdji et al., 2010; Gourdji et al., 2012)(Broquet et al., 2013;  
100 Gökede et al., 2010; Gourdji et al., 2010; Gourdji et al., 2012). Those Despite the uncertainties  
101 existing in regional inversions due to uncertainties in atmospheric transport, fossil fuel  
102 emissions, fire disturbance, and boundary conditions, these studies demonstrated do point to the  
103 possibility of comparing evaluating the spatiotemporal patterns of fluxes from biospheric models  
104 to those through the use of high resolution inverse models.

105 In With this paper, we propose a statistical model selection approach for using goal in mind, what  
106 is needed is an atmospheric-inversion-based method that can use variations in atmospheric CO<sub>2</sub>  
107 measurements to evaluate assess the spatiotemporal variability of patterns of surface carbon  
108 fluxes simulated by TBMs. The purpose of this paper is to present, evaluate, and demonstrate the  
109 application of such an approach, applied here to the evaluation of the 1°×1° and 3-hourly  
110 spatiotemporal variability of Net Ecosystem Exchange (NEE) at relatively fine scales (1°×1° and  
111 3-hourly resolution), in order to target scales at which the link between environmental drivers  
112 and simulated fluxes can inform TBM improvements. by TBMs using atmospheric CO<sub>2</sub>

113 measurements. This fine scale variability is evaluated here ~~across seasons (monthly) within each~~  
114 month and biomesbiome over North ~~American~~America, thus providing ~~an approach for~~  
115 ~~evaluating a way to evaluate~~ the seasonal and biome-specific differences in model performance.  
116 The distinguishing feature of the proposed approach is that it targets the evaluation of flux  
117 patterns at fine scales, rather than flux magnitudes at aggregated scales, thereby potentially  
118 providing a closer link to process-based understanding of TBM performance. The approach is  
119 first evaluated usingwith a series of synthetic data experiments, ~~followed by an~~ where the  
120 underlying flux patterns affecting the atmospheric CO<sub>2</sub> signals are known. The application ~~to of~~  
121 this approach is further tested and demonstrated using actual atmospheric measurements and a  
122 prototypical small set of extensively studied TBM simulations from the North American Carbon  
123 Program (NACP) Regional Interim Synthesis (RIS) effort (~~Huntzinger et al., 2012~~)(Huntzinger  
124 et al., 2012).

125 ~~The remainder of the paper is organized as follows. We describe the data used in the case~~  
126 ~~studies in Section 2. The proposed statistical model selection approach is introduced in Section~~  
127 ~~3. The experimental case studies are listed in Section 4. In Section 5, we evaluate the feasibility~~  
128 ~~of the proposed approach within the context of the information content of available atmospheric~~  
129 ~~observations using synthetic data experiments. In Section 6, we present the prototypical~~  
130 ~~application to evaluate four TBMs participating in the NACP RIS activities. Final conclusions~~  
131 ~~are presented in Section 7.~~

132



133 **2—Data description**

134 **2.1—Atmospheric CO<sub>2</sub> measurements**

135 ~~We use continuous, high-precision atmospheric CO<sub>2</sub> concentration measurements from 35~~  
136 ~~towers for the year 2008 (Shiga et al.) to evaluate the simulated NEE spatiotemporal variability~~  
137 ~~over North American land. The year 2008 is used as it includes the expansion of continuous~~  
138 ~~measurement locations from the Mid Continent Intensive (MCI) project (Miles et al., 2012; Ogle~~  
139 ~~et al., 2006). Atmospheric CO<sub>2</sub> measurements are processed as in Gourdji et al. (2012) and are~~  
140 ~~sub-selected as in Shiga et al. (submitted). To remove the effect of boundary conditions, we pre-~~  
141 ~~subtract the GLOBALVIEW CO<sub>2</sub> boundary condition from atmospheric measurements as in~~  
142 ~~Gourdji et al. (2012). This earlier study suggested that GLOBALVIEW CO<sub>2</sub> gives more~~  
143 ~~realistic estimate of CO<sub>2</sub> boundary conditions for North America relative to boundary conditions~~  
144 ~~taken from CarbonTracker. We further remove the impact of fossil fuel emissions by pre-~~  
145 ~~subtracting concentrations modeled based on the VULCAN ODIAC fossil fuel emissions~~  
146 ~~inventory (Shiga et al., submitted).~~

147 **2 Data description**

148 **2.1 Atmospheric CO<sub>2</sub> measurements**

149 We use continuous, high-precision atmospheric CO<sub>2</sub> concentration measurements from 35  
150 towers for the year 2008 to evaluate the simulated NEE spatiotemporal variability over North  
151 American land. Figure 1 shows the location of these towers along with the geographic coverage  
152 of seven North American biomes as modified from Olson et al. (2001). A majority of towers are  
153 located in Temperate Broadleaf and Mixed Forests, Temperature Grasslands, Savannas and  
154 Shrublands, Temperature Coniferous Forests and Boreal Forests and Taiga, while very few  
155 towers are located in the other biomes (Tundra, Desserts and Xeric, and Tropical and Subtropical

156 biomes). This distribution of towers is expected to affect the sensitivity of atmospheric CO<sub>2</sub> data  
157 to NEE within those biomes. The year 2008 is used as it includes the expansion of continuous  
158 measurement locations from the Mid-Continent Intensive (MCI) project (Miles et al., 2012; Ogle  
159 et al., 2006). Atmospheric CO<sub>2</sub> measurements are processed and averaged to 3-hourly intervals  
160 as described in Gourджи et al. (2012). Data from all hours of the day are used for tall towers with  
161 a height over 300m while afternoon data are used for most short towers (lower than 100m) and  
162 nighttime data are used for sites with complex topography (e.g. Niwot Ridge - NWR), as detailed  
163 in Shiga et al. (2014). We further remove data that are strongly influenced by only a few 1°×1°  
164 grid cells, in order to exclude data that are likely subject to systematic transport model errors  
165 (Göckede et al., 2010; Gourджи et al., 2012; Peters et al., 2007). The total number of resulting  
166 observations is  $n = 28,717$ .

167 To remove the effect of boundary conditions, we pre-subtract the GLOBALVIEW-CO<sub>2</sub>  
168 boundary condition (GLOBALVIEW-CO<sub>2</sub>, 2010) from atmospheric measurements as in Gourджи  
169 et al. (2012). We further remove the impact of fossil fuel emissions by pre-subtracting  
170 concentrations modeled based on the VULCAN-ODIAC fossil fuel emissions inventory (Shiga  
171 et al., 2014).

## 172 **2.2 Sensitivity footprints from atmospheric transport model**

173 The sensitivity of the available atmospheric observations (~~Section 2.1~~) to underlying CO<sub>2</sub> fluxes  
174 (in units of ppmv/( $\mu\text{mol m}^{-2}\text{s}^{-1}$ )) is quantified as described in Gourджи et al. (2012). In brief,  
175 footprints are derived from the Stochastic Time-Inverted Lagrangian Transport (STILT) model  
176 (~~Lin et al., 2003~~)(Lin et al., 2003), driven by meteorological fields from the Weather Research  
177 and Forecast (WRF) model (~~Skamarock and Klemp, 2008~~)(Skamarock and Klemp, 2008). The  
178 STILT transport model has been used and examined extensively at regional and continental

179 scales (~~Chatterjee et al., 2012; Gourджи et al., 2010; Gourджи et al., 2012; Huntzinger et al., 2011b;~~  
180 ~~Kort et al., 2008; McKain et al., 2012~~)(Chatterjee et al., 2012; Gourджи et al., 2010; Gourджи et al.,  
181 2012; Huntzinger et al., 2011; Kort et al., 2008; McKain et al., 2012). Footprints ~~can~~ also ~~be~~  
182 used to generate synthetic observational time series based on TBM flux simulations.

### 183 **2.3 Terrestrial Biospheric Models (TBMs)**

184 We ~~evaluate~~use simulations from four TBMs to evaluate the proposed approach, namely CASA-  
185 GFED (~~van der Werf et al., 2006~~)(van der Werf et al., 2006), SiB3 (~~Baker et al., 2008~~),  
186 ~~ORCHIDEE~~, SiB3 (Baker et al., 2008), ORCHIDEE (~~Krinner et al., 2005~~)(Krinner et al., 2005)  
187 and VEGAS2 (~~Zeng et al., 2005~~)(Zeng et al., 2005), using the runs submitted to the NACP RIS  
188 activity. These four models were selected for analysis because of the availability of 3-hourly  
189 NEE flux output. While CASA-GFED and VEGAS2 have a coarser native temporal resolution,  
190 their NEE fluxes have been downscaled to a 3-hourly resolution as described in ~~Huntzinger et al.~~  
191 ~~(2011b)~~Huntzinger et al. (2011). Our evaluation is based on the overall NEE simulated by each  
192 TBM, although model definitions of NEE differ: CASA-GFED includes fire disturbance while  
193 other models do not; ORCHIDEE exclude crop harvest while others do not. A comparison and  
194 summary of these simulations can be found in Table S1 in the supplementary material. Further  
195 details on the NACP RIS simulations can be found in Huntzinger et al. (~~2012~~)(2012).

### 196 ~~**3—Model selection based on Bayesian Information Criterion (BIC)**~~

### 197 **3 Regression framework linking atmospheric CO<sub>2</sub> to NEE**

198 The overall goal of the proposed approach is to evaluate the spatiotemporal variability of NEE as  
199 simulated by various TBMs using atmospheric CO<sub>2</sub> measurements. Such an approach must be  
200 based on an inverse model that can infer NEE from atmospheric CO<sub>2</sub> measurements. It must  
201 also include a statistical model selection component to evaluate the degree to which NEE

202 patterns predicted by TBMs are useful in explaining the observed atmospheric CO<sub>2</sub> variability.  
203 Rather than quantifying the magnitude of NEE, the primary goal here is to evaluate the  
204 spatiotemporal NEE patterns (at a 1°×1° and 3-hourly resolution) within specific biomes of  
205 North America and for specific months. The approach presented here builds on the geostatistical  
206 inverse modeling (GIM) framework (Gourdji et al., 2010; Gourdji et al., 2012; Michalak et al.,  
207 2004), but is presented here in the form of a regression analysis to simplify the presentation and  
208 emphasize the introduction of model selection aspect of the proposed approach.

209 To ~~do so~~to this end, we first formulate a multi-linear regression framework that relates atmospheric  
210 observations to NEE spatiotemporal variability. Statistical model selection is then applied to  
211 determine whether, when, and where the spatiotemporal variability of simulated NEE is  
212 consistent with that evident from variability in atmospheric CO<sub>2</sub>. Here, the NEE spatiotemporal  
213 variability is defined at a 1°×1° spatial and 3-hourly temporal resolution, and the TBMs are  
214 evaluated for within specific biome-month combinations. ~~The examined North American biomes~~  
215 ~~are shown in~~ Figure 4-2 shows the distribution of NEE in one specific biome-month combination  
216 (i.e., Boreal Forests and Taiga in July) as an example.

217 To link atmospheric measurement to surface fluxes we first define the observed atmospheric CO<sub>2</sub>  
218 concentrations, with the influence of boundary conditions and fossil fuel emissions pre-  
219 subtracted, as:

$$\mathbf{z} = \mathbf{H}\mathbf{s} + \boldsymbol{\varepsilon} \quad (1)$$

220 where  $\mathbf{z}$  is an  $n \times 1$  vector of atmospheric CO<sub>2</sub> observations,  $\mathbf{s}$  is an  $m \times 1$  vector of the  
221 ~~“true”~~underlying NEE fluxes at 1°×1° and 3-hourly resolution,  $\mathbf{H}$  ( $n \times m$ ) are the sensitivity  
222 footprints, namely a Jacobian matrix representing the sensitivity of each observation to each

223 underlying flux (i.e.,  $\frac{\partial z_t}{\partial s_j}$ ) as quantified using an atmospheric transport model (see Section 2.2),  
 224 and  $\boldsymbol{\epsilon}$  ( $n \times 1$ ) is the model-data mismatch term that represents any discrepancies between  
 225 observed ( $\mathbf{z}$ ) and modeled ( $\mathbf{H}\mathbf{s}$ ) CO<sub>2</sub> mixing ratios. The model-data mismatch term encompasses  
 226 the influence of errors in the boundary conditions, errors in the fossil fuel inventory,  
 227 representation errors, aggregation errors, transport model errors, and measurement errors. These  
 228 errors are assumed to have zero mean and be uncorrelated across measurements, with their  
 229 variances represented by a diagonal covariance matrix  $\mathbf{R}$  ( $n \times n$ ). The dimensions of the  
 230 matrices and vectors are based on the total number of observations,  $n = 28,717$ , and the total  
 231 number of fluxes at a  $1^\circ \times 1^\circ$  ( $2635$  such grid cells within the domain used here) and 3-hourly  
 232 resolution ( $366 \times 8 = 2928$ ) such periods within the span of the one-year inversion),  $m =$   
 233  $2635 \times 2928 = 7,715,280$ .  
 234 The spatiotemporal NEE distribution of  $\mathbf{s}$  is represented as a linear model of NEE as predicted  
 235 by various TBMs within specific biome-month combinations:

$$\mathbf{s} = \mathbf{X}\boldsymbol{\beta} + \boldsymbol{\xi} \quad (2)$$

236 where  $\mathbf{X}$  is a  $m \times p$  -matrix with each column representing NEE  $1^\circ \times 1^\circ$  3-hourly spatiotemporal  
 237 variability within a specific biome-month combination from a specific TBM, such that a given  
 238 column is populated by the modeled NEE from a given TBM for a given biome-month for those  
 239 rows (i.e. elements of  $\mathbf{s}$ ) corresponding to that specific biome-month combination, while the  
 240 remainder of the column is filled with zeros. These individual columns of  $\mathbf{X}$  are thus predictor  
 241 variables for the dependent variable  $\mathbf{s}$ . With 7 biomes (Figure 1) and 12 months, there are a total  
 242 of 84 possible predictor variables for each TBM- (i.e.,  $p \leq 84$  for one TBM). The  $p \times 1$  vector  $\boldsymbol{\beta}$   
 243 represents the drift coefficient describing the relationship between  $\mathbf{X}$  and  $\mathbf{s}$ , and  $\mathbf{X}\boldsymbol{\beta}$  together thus

244 represents a statistical model of the trend of NEE. The  $m \times 1$  vector  $\boldsymbol{\xi}$  represents the portion of  
245 the variability of  $\mathbf{s}$  that cannot be explained by the predictor variables in  $\mathbf{X}$ , and these deviations  
246 are modeled as having a mean of zero and a covariance matrix  $\mathbf{Q}$  ( $m \times m$ ) that represents how  
247 the flux deviations from the model of the trend (i.e.,  $\mathbf{s} - \mathbf{X}\boldsymbol{\beta}$ ) are correlated in time and space.

248 Combining these two equations, we represent the atmospheric observations  $\mathbf{z}$  in terms of the  
249 NEE predictor variables  $\mathbf{X}$ :

$$\mathbf{z} = \mathbf{HX}\boldsymbol{\beta} + \mathbf{H}\boldsymbol{\xi} + \boldsymbol{\varepsilon} \quad (3)$$

250 where  $\mathbf{z}$  is seen to have a spatiotemporally variable mean  $\mathbf{HX}\boldsymbol{\beta}$  and, assuming independence  
251 between  $\boldsymbol{\xi}$  and  $\boldsymbol{\varepsilon}$ , a residual covariance of:

$$\boldsymbol{\Sigma} = \mathbf{HQH}^T + \mathbf{R} \quad (4)$$

252 where  $T$  is the matrix transpose operation. From a statistical standpoint, our goal then becomes  
253 to select a subset of TBM biome-month combinations that ~~optimally represent~~capture a  
254 substantial portion of the  $\text{CO}_2$  variability ~~as~~-observed in  $\mathbf{z}$ . This constitutes a classical statistical  
255 model selection problem, in which we examine which predictor variables (candidate columns in  
256  $\mathbf{X}$ ) are useful in explaining the atmospheric  $\text{CO}_2$  measurements ( $\mathbf{z}$ ).

257 A widely applied approach for statistical model selection is the Bayesian Information Criterion  
258 (BIC) (Schwarz, 1978). BIC takes into account both the goodness of fit, i.e., the residual sum of  
259 squares ( $RSS$ ), and the numbers of auxiliary variables ( $k$ ) in each candidate model, and can be  
260 used to compare non-nested candidate models. BIC has also been adapted for use with  
261 spatiotemporally autocorrelated residuals (~~Hoeting et al., 2006; Mueller et al., 2010~~)(Hoeting et  
262 al., 2006; Mueller et al., 2010) and within the context of atmospheric inversions where  
263 atmospheric observations are used to inform underlying surface fluxes (~~Gourdji et al.,~~

264 | ~~(2012)~~(Gourdji et al., 2012), making it ideal for the application presented here. The standard  
 265 | expression for BIC is:

$$BIC = \underbrace{\ln|\Sigma| + RSS}_{\text{log likelihood}} + \underbrace{k \ln(n)}_{\text{penalty term}} \quad (5)$$

266 | where  $RSS$  represents the residual sums of squares of a given candidate model  $\mathbf{X}_c$ ,  $\Sigma$  is the  $n \times n$   
 267 | covariance matrix of the residuals (Eq. 4),  $||$  denotes the matrix determinant, and  $k$  is the number  
 268 | of parameters in a particular candidate model. For the specific application presented here (Eq. 1-  
 269 | 4) and factoring out the unknown drift coefficients,  $\beta$  and  $RSS$  become as in ~~Gourdji et al.~~  
 270 | ~~(2012)~~Gourdji et al. (2012):

$$\beta = ((\mathbf{H}\mathbf{X}_c)^T \Sigma^{-1} (\mathbf{H}\mathbf{X}_c))^{-1} (\mathbf{H}\mathbf{X}_c)^T \Sigma^{-1} \mathbf{z} \quad (6)$$

$$RSS = \left[ \mathbf{z}^T \left( \Sigma^{-1} - \Sigma^{-1} (\mathbf{H}\mathbf{X}_c) ((\mathbf{H}\mathbf{X}_c)^T \Sigma^{-1} (\mathbf{H}\mathbf{X}_c))^{-1} (\mathbf{H}\mathbf{X}_c)^T \Sigma^{-1} \right) \mathbf{z} \right] \quad (7)$$

271 | The specific covariance parameters needed to define  $\mathbf{Q}$  and  $\mathbf{R}$ , which are ~~themselves~~ needed to  
 272 | define  $\Sigma$ , vary between experiments and are obtained as described in the supplementary  
 273 | materials.

274 | ~~The~~Model selection built on this framework aims to identify the “best” model of the trend based  
 275 | on a tradeoff between model size and the model’s power in explaining the variations in observed  
 276 | atmospheric CO<sub>2</sub>. Here, the “best” model is specially defined as ~~that one~~ with the minimum BIC  
 277 | value, ~~thus~~ providing an optimal balance between model complexity and model fit. To identify  
 278 | this model, BIC is compared across all possible combinations of predictor variables (i.e. 84 NEE  
 279 | biome-months per TBM). Due to the large number of candidate predictor variables considered  
 280 | here, we implement the branch-and-bound algorithm of Yadav et al. ~~(2013)~~(2013) to improve  
 281 | computational efficiency.

282 The final selected subset of TBM biome-months represents those biomes and months within  
283 which a given TBM exhibits spatiotemporal variability that explains a substantial portion of the  
284 variability observed in the observations  $\mathbf{z}$  (see Eq. 3). For a given TBM biome-month  
285 distribution to be “selected” as part of the “best” model of the trend, therefore, (1) the available  
286 atmospheric observations must be sensitive to the spatiotemporal variability of fluxes within that  
287 biome-month (as represented through  $\mathbf{H}$ ), i.e., the information contained in atmospheric data  
288 sufficiently constrains the spatiotemporal variability within that biome-month, and (2) the  
289 variability within a particular biome-month as represented by a particular TBM must explain a  
290 sufficient portion of the variability in the atmospheric observations to offset the penalty term in  
291 Eq. (5), i.e. the reduction in  $RSS$  must outweigh the penalty term. On the contrary, if a given  
292 TBM biome-month distribution is “not selected” then, either (1) or (2) as given above is not  
293 satisfied, i.e., either that atmospheric observations are not sensitive to the NEE variability within  
294 that biome-month, or that the NEE variability as represented in the model is inconsistent with  
295 atmospheric observations. In other words, selecting or not selecting a TBM biome-month  
296 combination directly reflects on the performance of the TBM in that biome and month, as long as  
297 we have fulfilled the requirement in (1) above. If the condition in (1) is not met, we are not able  
298 to use the model selection results to examine model performance, due to the insufficient  
299 coverage of the network. We henceforth refer to the TBM biome-month combinations included  
300 in the final selected subset as the “selected” combinations or elements, or alternately as the TBM  
301 biome-month combinations “identified” using the atmospheric data.

#### 302 **4 Synthetic data and real data experiments**

303 In this Section, we design a series of Synthetic Data (SD) experiments (Figure 23), in which the  
304 underlying fluxes are prescribed, to ~~test the proposed approach and~~ assess the ~~degree to which~~



305 ~~current sensitivity of atmospheric observations are sensitive to, and informative of, the CO<sub>2</sub>~~  
306 ~~measurements to NEE flux spatiotemporal variability of NEE patterns within all biome-month~~  
307 ~~combinations, and identify when and where results from the proposed approach reliably reflect~~  
308 ~~model performance in simulating NEE spatiotemporal variability.~~ We further introduce two Real  
309 Data (RD) experiments as a proof-of-concept demonstration of our approach. In those RD  
310 experiments, we use actual atmospheric CO<sub>2</sub> measurements to evaluate the spatiotemporal  
311 variability of NEE as simulated by ~~the~~ four prototypical TBMs ~~described in~~ (Section 2.3-).

312 In the SD experiments, synthetic atmospheric observations ( $\mathbf{z}$ ) are generated as described in Eq.  
313 (1) using fluxes ( $\mathbf{s}_{\text{TBM}}$ ) that include NEE as simulated by one of the TBMs and, in some cases,  
314 spatiotemporally-correlated flux residuals ( $\xi$ ) and model-data mismatch errors ( $\epsilon$ ), *i.e.*,  $\mathbf{z} =$   
315  $\mathbf{H}(\mathbf{s}_{\text{TBM}} + \xi) + \epsilon$ . The superset of candidate ancillary variables (Figure 23,  $\mathbf{X}$ ) includes NEE  
316 from one or more TBMs. TBMs included in  $\mathbf{s}_{\text{TBM}}$  and  $\mathbf{X}$  are denoted as the “truth” and the  
317 “candidate (s)” respectively henceforth.

318 The first SD case study, SD-one-ØØ (Figure 23), is designed to investigate whether, when, and  
319 where the information contained in current atmospheric data enables the identification of the  
320 correct candidate TBM for a case where it is the only TBM considered in the model selection,  
321 where this TBM fully represents the variability in the synthetic atmospheric observations ( $\xi=0$ ),  
322 and where no model-data mismatch errors are included in the simulation ( $\epsilon=0$ ). Given that in this  
323 case the candidate TBM explains all of the variability in the synthetic atmospheric observations,  
324 it should always be selected if the atmospheric data are sufficiently sensitive to NEE across all  
325 biome-months; hence, biome-months for which the TBM is not selected are ones to which the  
326 atmospheric CO<sub>2</sub> observations are not sufficiently sensitive to offset the penalty term in Eq. (5).

327 The second and third SD case studies, SD-one- $\emptyset\epsilon$  and SD-one- $\xi\epsilon$  (Figure 23), are analogous to  
328 SD-one- $\emptyset\emptyset$ , but include model-data mismatch errors ( $\epsilon \neq 0$ , denoted by  $\epsilon$ ) and/or spatially  
329 correlated flux residuals ( $\xi \neq 0$ , denoted by  $\xi$ ). These case studies are designed to test the degree  
330 to which current atmospheric observations can inform the spatiotemporal variability of NEE in  
331 cases with realistic model-data mismatch errors and where the candidate TBM only represents a  
332 portion of the true underlying NEE variability. ~~The details of the model-data mismatch errors~~  
333 ~~and flux residuals are described~~In these case studies, noise ( $\epsilon$ ) is added to observations,  
334 generated as a random vector of independent normally-distributed values with variances  
335 corresponding to the diagonal elements of  $\mathbf{R}$ , which are inferred from the RD-all- $\xi\epsilon$  experiment  
336 (described below), and a mean of 0. In addition for SD-one- $\xi\epsilon$ , the flux signal from the TBMs is  
337 augmented with additional spatially-correlated fluxes ( $\xi$ ) generated as a random vector of  
338 normally distributed values with a covariance structure equal to that inferred from the RD-all- $\xi\epsilon$   
339 experiment (described below). The details of the model-data mismatch errors and flux residuals  
340 are summarized in the supplementary materials.

341 The final SD case study, SD-all- $\xi\epsilon$ , builds on SD-one- $\xi\epsilon$  (Figure 23), but is designed to test  
342 whether the correct TBM can be identified when all four TBMs are used as candidate variables.  
343 This case study therefore explores whether current atmospheric observations can be used to  
344 differentiate among candidate TBMs. No constraints are placed on the model selection, such that  
345 more than one TBM can be selected for the same biome-month, but only the dominant TBM (i.e.  
346 the one with the largest  $\beta$ , Eq. 6) is discussed in analyzing this case.

347 Finally, two RD case studies, RD-one- $\xi\epsilon$  and RD-all- $\xi\epsilon$ , are defined analogously to SD-one- $\xi\epsilon$   
348 and SD-all- $\xi\epsilon$ , to ~~examine~~further test the applicability of our approach by examining the actual  
349 performance of the four prototypical TBMs based on available atmospheric observations. The

350 observations ( $\mathbf{z}$ ) here are the actual atmospheric measurements, which by definition encompass  
351 model-data mismatch errors, and the flux residuals are also inherently present as no TBM is  
352 expected to perfectly reflect the true underlying fluxes. In each RD-one- $\xi\epsilon$  experiment, one of  
353 the four prototypical TBMs is used as the candidate TBM in order to assess individual TBM  
354 performance. In RD-all- $\xi\epsilon$ , all four TBMs are included, analogously to SD-all- $\xi\epsilon$ , to identify the  
355 TBM (if any) that best represents the spatiotemporal variability of NEE within a given biome-  
356 month, based on the information provided by the atmospheric measurements.

## 357 **5 Sensitivity of atmospheric observations to NEE flux—spatiotemporal** 358 **variability and evaluation of the proposed approach**

359 The SD-one- $\emptyset\emptyset$  experiment examines the sensitivity of atmospheric observations to underlying  
360 flux variability and evaluates the proposed approach under idealized conditions where the true  
361 flux field is perfectly represented by the candidate TBM model, and where no model-data  
362 mismatch errors are included in the synthetic atmospheric observations.

363 Results indicate that the candidate TBM is selected for over 90% of all biome-months (Figure  
364 34, top row), demonstrating that atmospheric observations are sensitive to NEE spatiotemporal  
365 variability, and that the proposed ~~model-selection~~ approach leverages this sensitivity to correctly  
366 identify the TBM model as being representative of the flux variability- within the vast majority  
367 of biomes and months. The only notable exception is for the Tundra biome for which, other than  
368 during the height of the growing season, the atmospheric data do not provide a sufficient  
369 constraint on the flux variability, due to the poor data coverage and the weak biospheric signal.

370 Because this biome ~~plays~~ is expected to play an important role in ~~the future~~ global carbon cycle  
371 and climate (~~Belshe et al., 2013; Ping et al., 2008; Schuur et al., 2009; Tarnocai et al.,~~  
372 ~~2009~~) (Belshe et al., 2013; Ping et al., 2008; Schuur et al., 2009; Tarnocai et al., 2009) and large  
373 uncertainties remain in quantifying its role ~~and evolution with time~~ in carbon cycling (~~McGuire et~~

374 | ~~et al., 2012~~(McGuire et al., 2012), this result highlights the need for strategic placement of  
375 | additional CO<sub>2</sub> monitoring stations in the vicinity of this biome to constrain its carbon flux  
376 | distribution.

377 | The SD-one- $\emptyset\epsilon$  and SD-one- $\xi\epsilon$  case studies examine the degree to which the presence of model-  
378 | data mismatch errors and ~~a portion of additional~~ flux variability not represented by the candidate  
379 | TBM limit the information content of available observations, and the ability of the proposed  
380 | approach to observe the spatiotemporal flux variability under more realistic conditions identify  
381 | the consistency between the true underlying NEE patterns and those simulated by TBMs.

382 | Results of SD-one- $\emptyset\epsilon$  show that including realistic model-data mismatch errors decreases the  
383 | information content of atmospheric observations to the point where a TBM that in reality  
384 | represents the full spatiotemporal flux variability is not selected for many ~~month TBM~~  
385 | ~~combinations in months and TBMs within~~ the Tropical and Subtropical biome, as well as the  
386 | Desert and Xeric Shrublands biome, in addition to the Tundra biome that was not well  
387 | constrained even under idealized conditions (Figure 34, middle row). The identification of a  
388 | TBM as correctly representing the flux ~~variability patterns~~ also becomes more challenging during  
389 | winter and spring ~~overwithin~~ the Boreal Forests and Taiga biome, and the Temperate Coniferous  
390 | Forests biome (Figure 34, middle row), especially when VEGAS2 is used as the true flux  
391 | distribution. This result is related to the fact that the magnitude and the spatiotemporal  
392 | variability of NEE simulated by VEGAS2 ~~overwithin~~ those biome-months are much smaller than  
393 | for other TBMs. For example, the standard deviation of NEE simulated by VEGAS2 is less than  
394 | a half of that of other TBMs. Overall, the inclusion of realistic model-data mismatch, combined  
395 | with the coverage of the monitoring network, make the identification of TBMs that represent the  
396 | spatiotemporal variability of fluxes within biomes unreliable ~~overfor~~ three of the seven biomes

397 considered here, namely the Tundra, Tropical and Subtropical, and Desert and Xeric Shrublands  
398 biomes. Subsequent analyses therefore focus on the remaining four better-constrained biomes,  
399 namely the (i) Boreal Forests and Taiga, (ii) Temperate Coniferous Forests, (iii) Temperate  
400 Grasslands, Savannas, and Shrublands, and (iv) Temperate Broadleaf and Mixed Forests biomes.

401 SD-one- $\xi\epsilon$  is ~~designed as~~ the most realistic single-TBM synthetic data experiment, as it includes  
402 not only model-data mismatch errors, but also variability in the spatiotemporal flux distribution  
403 that is not represented by the candidate TBM. Results for the better-constrained biomes indicate  
404 that the ability to identify a model as correctly representing a portion of the true flux variability  
405 deteriorates in the winter months for the Boreal Forests and Taiga, but remains largely  
406 unchanged in the other biomes (Figure 34, bottom row). For the winter in the Boreal Forests and  
407 Taiga biome, the TBM is only identified when the fluxes are based on SiB3, likely because this  
408 TBM has a stronger flux signal in this biome during the winter relative to the other TBMs,  
409 thereby overcoming the confounding impacts of model-data mismatch errors and additional flux  
410 variability unexplained by the TBM. ~~Overall, however, results~~

411 Results of SD-one- $\xi\epsilon$  indicate that, under realistic conditions, the proposed approach ~~combined~~  
412 ~~with the available atmospheric observations are is~~ able to correctly identify a TBM that ~~correctly~~  
413 represents a portion of the true underlying flux variability ~~for much of the year over within~~ four  
414 of the seven biomes considered here-, given the monitoring network used here. The magnitude  
415 of the model data mismatch used here was derived from the real-data experiments (RD-one-  $\xi\epsilon$ ),  
416 and includes the impact of errors in the transport model, boundary conditions, fossil fuel  
417 emissions, and fire emissions, as well as measurement and aggregation errors. Therefore, results  
418 suggest that conclusions over the four considered biomes are robust in spite of the influences of  
419 those uncertainties. We acknowledge that the errors applied do not fully address the complexity

420 of uncertainties in the real world, as we assume that errors are independent and follow a  
421 Gaussian distribution. However, the results presented here, together with evidence from the  
422 literature (e.g., Gourdji et al., 2012; Pillai et al., 2012), support the ability to infer flux patterns  
423 despite the many sources of uncertainty in regional inversions.

424 The final SD case, SD-all- $\xi\epsilon$ , is designed to explore whether atmospheric observations can be  
425 used to differentiate among several competing TBMs to identify the TBM that best represents the  
426 underlying flux variability. Results indicate that across the majority of the examined biomes,  
427 months, and TBMs, the proposed approach combined with the available atmospheric data are  
428 able to discriminate among models for a similar fraction of TBM-biome-month combination  
429 (Figure 45) as when only the “correct” TBM was offered as a candidate model (SD-one- $\xi\epsilon$ ,  
430 Figure 34, bottom row).

431 One noticeable difference, however, occurs during the growing season in the Boreal Forests and  
432 Taiga when VEGAS2 or CASA-GFED is used to represent a substantial portion of the true flux  
433 variability. In these cases, the other of these two models is often identified in the model  
434 selection procedure. This is not surprising, because these two models yield fluxes that are highly  
435 spatiotemporally correlated to one another (Figure 56), and because biospheric signals simulated  
436 by VEGAS2 are particularly weak (Huntzinger et al., 2011b),(Huntzinger et al., 2011). Overall,  
437 therefore, for the four better-constrained biomes, the information content of the atmospheric data  
438 is sufficient to identify a TBM that represents a substantial portion of the true underlying  
439 variability using the proposed approach, even when multiple competing TBMs are available. In  
440 other words, atmospheric observations can be used to differentiate among competing TBMs.  
441 The exception, not surprisingly, is when the competing TBMs have fluxes that are highly  
442 correlated ( $R>0.8$ ), which, for the four TBMs examined here, occurs most often over the Boreal

443 Forests and Taiga and Temperate Coniferous Forests biomes (where biospheric signals are  
444 relative weak and atmospheric data are less sensitive), for the VEGAS2 and CASA-GFED as  
445 well as SiB3 and ORCHIDEE model pairs (Figure 56).

446 ~~6—Evaluation Demonstration of NACP-RIS simulations in representing NEE~~  
447 ~~spatiotemporal variability~~

448 ~~6 Section 5 confirms that the proposed model selection approach, combined~~  
449 ~~with available CO<sub>2</sub> measurements, using atmospheric observations~~

450 ~~The results presented in Section 5 confirm that, given the coverage of atmospheric data available~~  
451 ~~in 2008, the proposed approach~~ is able to identify TBMs representing a substantial portion of the  
452 underlying NEE spatiotemporal variability over ~~4four~~ better-constrained biomes of North  
453 America ~~largely~~ throughout ~~most of the~~ year. In this Section, by focusing on the RD  
454 experiment results, we ~~examine the performance of~~ demonstrate the application of the proposed  
455 approach using “real” data, by evaluating four prototypical TBMs participating in the NACP  
456 RIS.

457 **6.1 Performance of TBMs in simulating the spatiotemporal variability of NEE, as**  
458 **assessed using atmospheric CO<sub>2</sub> measurements**

459 The RD-one- $\xi\epsilon$  case study includes ~~4four~~ experiments, each evaluating one prototypical TBM.  
460 As a general indication of individual TBM performance across biomes and months, we sum the  
461 number of candidate TBMs selected across the four RD-one- $\xi\epsilon$  cases (Figure 6). ~~Overall, we~~  
462 We find that the capability of TBMs to simulate the NEE spatiotemporal variability varies  
463 strongly across biomes and seasons. TBMs are most frequently identified over the Temperate  
464 Broadleaf and Mixed Forests biome (7 out of 12 months with at least one TBM identified), and  
465 least frequently identified over the Boreal Forests and Taiga biome (3 out of 12 months with at  
466 least one TBM identified). Across seasons, TBMs are most frequently identified during the  
467 growing season (May-Sept, 15 out of 20 biome-months with at least one TBM identified). TBMs

468 are least frequently identified during transition seasons (Mar-Apr and Oct-Nov, with 2 out of 16  
469 biome-months with at least one TBM identified), likely reflecting known challenges of TBMs in  
470 representing the seasonal cycle of phenology (~~Richardson et al., 2012; Schaefer et al., 2012;~~  
471 ~~Schwalm et al., 2010~~)(Richardson et al., 2012; Schaefer et al., 2012; Schwalm et al., 2010).  
472 Specifically, during Oct-Nov, none of the TBMs is identified as representing the flux  
473 spatiotemporal variability in any of the biomes, in agreement with the finding in ~~Gourdji et al.~~  
474 ~~(2012)~~Gourdji et al. (2012) that carbon fluxes simulated by over 70% of the NACP TBMs are  
475 outside the 95% confidence intervals of atmospheric inversion estimates in October.

476 Of all 48 biome-months examined, none of the four TBMs are identified as substantially  
477 representing the spatiotemporal variability ~~in~~within 27 biome-months, and only one TBM is  
478 identified in 5 additional biome-months (Figure 67). Multiple TBMs are identified as  
479 representing a portion of the spatiotemporal variability ~~in~~within the remaining 16 biome-months  
480 (Figure 67). Interestingly, SiB3 and ORCHIDEE are selected in almost all of these 16 biome-  
481 months, suggesting that they both have the potential to explain a substantial portion of the  
482 observed variability in atmospheric CO<sub>2</sub>. This is consistent with the similarity in NEE  
483 spatiotemporal series between SiB3 and ORCHIDEE shown in Figure 56.

484 The RD-all-~~ξε~~ case study identifies the TBM that best represents the underlying flux variability  
485 (Figure 7). ~~Over the 16 biome months for which more than one TBM was selected in the RD-~~  
486 ~~one-ξε series of experiments, SiB3 is identified as the dominant model explaining the observed~~  
487 ~~atmospheric CO<sub>2</sub> variability for 10 biome months, ORCHIDEE is identified over 4 biome-~~  
488 ~~months, while CASA GFED2 is identified over the remaining 2 biome months (Figure 7). For~~  
489 ~~the 5 biome months with only one TBM selected in the RD one-ξε series of experiments, the~~  
490 ~~selected TBM is consistent in the RD all-ξε experiment, with 3 biome months best represented~~



491 ~~by SiB3 and 2 others by ORCHIDEE. Furthermore, out8). Out~~ of 27 biome-months for which  
492 no individual TBM was selected in the RD-one-~~ξξ~~ experiments, 5 biome-months lead to models  
493 being selected when more than one model can be used in combination, with the dominant TBM  
494 being ORCHIDEE over the Temperate Coniferous Forests biome in Apr and May and the  
495 Temperate Broadleaf and Mixed Forests in Feb, SiB3 over the Boreal Forests and Taiga in Aug,  
496 and VEGAS2 over the Temperate Grasslands, Savannas and Shrublands in Dec.

497 Overall, SiB3 and ORCHIDEE are selected as the dominant TBM in explaining the flux  
498 variability as observed through the atmospheric CO<sub>2</sub> measurements more often than VEGAS2  
499 and CASA-GFED (Figure ~~78~~). SiB3 appears most representative of flux patterns over boreal  
500 biomes, whereas ORCHIDEE is most representative over temperate biomes. Although SiB3  
501 appears to be selected most often (13 biome-months), followed by ORCHIDEE (10 biome-  
502 months), none of the TBMs is consistently better than the others across all biomes and seasons.

## 503 6.2 Discussion~~Evaluation~~ of the TBMs and the proposed approach within the context of 504 earlier studies

505 ~~To further evaluate the performance of, and value added provided by, the proposed approach, we~~  
506 ~~assess the RD-one- ξξ results within the context of the existing literature to determine whether~~  
507 ~~(1) results are consistent with the literature wherever they are comparable, and (2) the proposed~~  
508 ~~approach can provide insights that go beyond those provided by other model evaluation~~  
509 ~~strategies.~~ Many of our findings are consistent with early work analyzing the examined TBMs

510 ~~We within the framework of the NACP RIS. For example, we~~ find distinctive seasonal  
511 differences in TBM performance in simulating ~~spatiotemporal flux variability (NEE~~ (Figures ~~6~~  
512 ~~and 7 and 8~~), consistent with the previously noted model misrepresentation of phenology  
513 ~~seasonality~~ based on site-level measurements (~~Richardson et al., 2012; Schaefer et al., 2012;~~

514 ~~Schwalm et al., 2010~~(Richardson et al., 2012; Schaefer et al., 2012; Schwalm et al., 2010);  
515 ~~These model limitations~~. In addition, we find that models perform better for Temperate  
516 Broadleaf and Mixed Forests, and that SiB3 appears to be more consistent with observations than  
517 other models, both of which are consistent with existing literature evaluating NACP RIS models  
518 (Raczka et al., 2013; Schwalm et al., 2010). The consistency between our results and existing  
519 literature further supports the performance of the proposed approach. It also implies that,  
520 although the approach proposed here is subject to many of the same uncertainties in fossil fuel  
521 emissions, fire disturbance, boundary conditions and transport models that affect all regional  
522 inversions, the main conclusions regarding TBM performance for the four major biomes  
523 examined here are quite robust.

524 The proposed approach also provides the opportunity to draw conclusions that go beyond the  
525 current literature. We present two examples here.

526 First, results indicate that model capability in simulating the spatiotemporal variability (i.e.  
527 patterns) of NEE varies strongly with seasons, with greater skill during the growing season than  
528 during the transition seasons. In other words, even within specific biomes and months, the  
529 variability of NEE is better represented during the growing season. This seasonal variability in  
530 model performance may be due to seasonal differences in the dominant environmental drivers  
531 controlling the ~~NEE~~spatiotemporal variability of NEE. For example, ~~Mueller et al.~~  
532 ~~(2010)~~Mueller et al. (2010) found that site-level NEE measurements the environmental drivers  
533 controlling NEE at one location were best explained by a hardwood forest vary across seasons,  
534 with radiation, nighttime temperature and vegetative radiation indices (i.e., fPAR) dominating  
535 during the growing, non-growing and leaf-out seasons, respectively. We hypothesize that the  
536 seasonal ~~difference~~differences in model performance is likely related to the models' ability to

537 represent the seasonally-varying influence of such environmental drivers. ~~As our results are~~  
538 ~~based on~~Because the NEE spatiotemporal variability, ~~which has been showed to be is~~ directly  
539 related to environmental processes and drivers (Beer et al., 2010; Mueller et al., 2010; Yadav et  
540 al., 2012; Gourdji et al., 2012), ~~our work allows a potential further the proposed approach~~  
541 provides a close link between model performance and environmental processes ~~to test this~~  
542 ~~hypothesis.~~  
543 ~~We also~~Second, we find that SiB3 and ORCHIDEE are identified more often as representing the  
544 spatiotemporal flux variability than VEGAS2 and CASA-GFED. ~~Overall, SiB3 and~~  
545 ~~ORCHIDEE can both explain a substantial portion of the observed variability over almost all of~~  
546 ~~the 16 biome months for which multiple TBMs are selected in the RD one  $\xi$  experiments~~  
547 ~~(Figure 6).~~ Given that the simulated NEE spatiotemporal variability is more similar between  
548 SiB3 and ORCHIDEE, and between VEGAS2 and CASA-GFED, relative to across these two  
549 model pairs (Figure 56), this finding suggests that aspects of the model internal structure  
550 common within the pairs likely contribute to similarities in simulated ~~fluxes~~flux patterns and  
551 associated performance. ~~As shown in Table S1 in the supplementary material, those~~Such features  
552 include: 1) SiB3 and ORCHIDEE use Enzyme Kinetic (EK) models while CASA-GFED2 and  
553 VEGAS use Light Use Efficiency (LUE) models to formulate their photosynthesis processes; 2)  
554 the native model time step of SiB3 and ORCHIDEE is shorter than a day while that of CASA-  
555 GFED and VEGAS2 varies from daily to monthly; and 3) SiB3 and ORCHIDEE have  
556 substantially more plant functional types (PFTs) than CASA-GFED and VEGAS2. ~~Schaefer et~~  
557 ~~al. (2012) suggested that EK and LUE models can perform equally well in simulating fluxes,~~  
558 ~~making this difference a less likely differentiating factor for performance between the two model~~  
559 ~~pairs. Native model time step, on the other hand, has been shown by Schwalm et al. (2010) to be~~

560 ~~an important factor affecting model performance. Finally, using fewer PFTs limits flux~~  
561 ~~variability to larger scales, as indicated in Huntzinger et al. (2011a) who found that NEE~~  
562 ~~simulated by SiB3 has greater variance and smaller correlation length scales than CASA GFED.~~  
563 ~~Model biases may arise from using uniform parameters within a limited number of PFTs that~~  
564 ~~leads to flux variability at larger scales, while actual processes may vary strongly within each~~  
565 ~~PFT and the actual fluxes vary at small scales (Schaefer et al., 2012; Schwalm et al., 2010).~~  
566 ~~Therefore, we hypothesize that the fewer PFTs and daily monthly time steps in CASA GFED~~  
567 ~~and VEGAS2 may explain their relatively poorer performance in simulating NEE spatiotemporal~~  
568 ~~variability relative to SiB3 and ORCHIDEE. Although it is not possible to draw definite~~  
569 ~~conclusions about the links between model structure and model performance in simulating flux~~  
570 ~~patterns based on the small number of TBMs examined here and the lack of a uniform simulation~~  
571 ~~protocol, a future application of this approach to a larger ensemble of models following a~~  
572 ~~uniform protocol would make it possible to explore these connection in more detail.~~

## 573 **7 Concluding remarks**

574 In this paper, we ~~develop~~present, evaluate and demonstrate a statistical ~~model selection~~  
575 ~~using~~based on GIM and the Bayesian Information Criterion to evaluate the spatiotemporal  
576 variability of net ecosystem exchange (NEE) as simulated by TBMs, against atmospheric CO<sub>2</sub>  
577 concentration measurements from 35 towers in North America in 2008. ~~We apply~~We  
578 ~~demonstrate the applicability of this method to evaluate~~demonstrate the applicability of this  
579 ~~approach by evaluating~~ 4 prototypical  
580 TBMs participating in the North American Carbon Program Regional Interim Synthesis (NACP  
581 RIS).

581 We first design a series of synthetic data experiments in which the underlying fluxes are  
582 prescribed, to test the proposed approach and examine whether, when, and where atmospheric

583 measurements are sensitive to, and hence can constrain, the spatiotemporal variability simulated  
584 by different TBMs. We find that due to the poor data coverage and weaker biospheric signals,  
585 current atmospheric observations cannot be used to reliably assess the flux spatiotemporal  
586 variability in the Tundra, Desert and Xeric Shrublands, and Tropical and Subtropical biomes.  
587 The remaining four biomes (i.e., Temperate Broadleaf and Mixed Forests, Temperate  
588 Grasslands, Savannas and Shrublands, Boreal Forests and Taiga, and Temperate Coniferous  
589 Forest), however, are found to be well constrained by atmospheric data. Over these four biomes,  
590 the synthetic data experiments suggest that the proposed model selection approach, combined  
591 with the available atmospheric data, are able to identify the TBMs that represent a substantial  
592 portion of the underlying flux variability, as well as differentiate among multiple competing  
593 TBMs.

594 ~~When~~We further test and demonstrate the application of the approach by evaluating the  
595 performance of four prototypical TBMs that have been extensively assessed in literature using  
596 ~~available~~actual atmospheric observations,~~we.~~ We find that ~~TBM~~conclusions about model  
597 performance ~~in simulating NEE spatiotemporal variability varies strongly across seasons and~~  
598 ~~biomes are consistent with existing literature for cases where results are comparable, further~~  
599 supporting the applicability of our approach. Those results include that 1) TBMs represent fine-  
600 scale flux spatiotemporal variability fluxes best during the growing season (May-September) and  
601 least consistently with atmospheric observations during the transition seasons, especially in  
602 October and November.~~Regionally,; and that 2) TBMs appear to perform best over the~~  
603 Temperate Broadleaf and Mixed Forests biome,~~and least well over.~~ The experiments performed  
604 here also lead to new conclusions about the ~~Boreal Forests and Taiga biome.~~ ~~None of~~  
605 ~~the examined~~ TBMs ~~evaluated is consistently better than the other TBMs across biomes and~~

606 ~~seasons, although. For example, results show that~~ SiB3 and ORCHIDEE appear to represent the  
607 flux variability ~~across more biome within individual biomes and~~ months ~~better~~ relative to  
608 CASA-GFED and VEGAS2.

609 ~~The spatiotemporal variability of carbon fluxes can be related to~~In addition, this approach has the  
610 potential to link model ~~internal structure and~~performance with environmental processes ~~(Beer et~~  
611 ~~al., 2010; Mueller et al., 2010; Yadav et al., 2012; Gourdji et al., 2012), and our work therefore~~  
612 ~~highlights some potential linkages between model performances and structure/processes. We~~  
613 ~~find distinctive, making it possible to test the hypothesis that~~ seasonal differences in TBM  
614 performance, ~~and hypothesize that these may~~ reflect models' ability to represent the seasonal  
615 variability in the dominant environmental controls on fluxes. ~~Future work will be conducted to~~  
616 ~~explore the connection between environmental processes and model performance. In addition,~~  
617 ~~we find that models with more PFTs and shorter native time steps may have an advantage in~~  
618 ~~simulating fine scale flux patterns. It must be noted, however, that the comparison conducted~~  
619 ~~here only included four TBMs, and that these TBMs were not run using a uniform experimental~~  
620 ~~protocol (Huntzinger et al., 2012), therefore making the link between model performance and~~  
621 ~~model structure preliminary at this stage. Repeating the analysis across a larger ensemble of~~  
622 ~~models following a uniform protocol ensemble represents another logical next step.~~

623 The comparison conducted here only included four TBMs, and was intended primarily as a  
624 demonstration of the proposed approach. Furthermore, these four TBMs were not run using a  
625 uniform experimental protocol (Huntzinger et al., 2012), precluding any conclusive results about  
626 linkages between model performance and model structure. Applying the approach presented  
627 here to a larger ensemble of models, ideally following a uniform simulation protocol, therefore  
628 represents a logical next step.

629 **Acknowledgments**

630 The authors thank the biospheric modelers participating the NACP Regional Interim Synthesis,  
631 and specifically Ning Zeng, Ian Baker, Nicolas Viovy, and James Randerson who provided the  
632 model results used in the analysis presented here. We thank Deborah Huntzinger for downscaling  
633 the CASA-GFED and VEGAS2 fluxes to 3-hourly temporal resolution. Atmospheric and  
634 Environmental Research (AER), and in particular Thomas Nehrkorn, John Henderson, and  
635 Janusz Eluszkiewicz, performed the WRF-STILT simulations and provided the sensitivity  
636 footprints. We acknowledge various data providers for the continuous in-situ CO<sub>2</sub> measurements,  
637 as well as Sharon Gourdji and Kim Mueller for their earlier efforts in collecting and processing  
638 those datasets. This work is funded by the National Aeronautics and Space Administration  
639 (NASA) under Grant No. NNX12AB90G- [and No. NNX12AM97G](#).

640

641 **Reference**

- 642 Baker, I., Denning, A. S., Hanan, N., Prihodko, L., Uliasz, M., Vidale, P.-L., Davis, K., and  
643 Bakwin, P.: Simulated and observed fluxes of sensible and latent heat and CO<sub>2</sub> at the  
644 WLEF-TV tower using SiB2.5, *Global Change Biology*, 9, 1262-1277, 2003.
- 645 Baker, I. T., Prihodko, L., Denning, A. S., Goulden, M., Miller, S., and Da Rocha, H. R.:  
646 Seasonal drought stress in the Amazon: Reconciling models and observations, *Journal of*  
647 *Geophysical Research: Biogeosciences*, ~~113, G00B01~~ [doi: 10.1029/2007JG000644](#),  
648 2008-.
- 649 Balzarolo, M., Boussetta, S., Balsamo, G., Beljaars, A., Maignan, F., Calvet, J. C., Lafont, S.,  
650 Barbu, A., Poulter, B., Chevallier, F., Szczypta, C., and Papale, D.: Evaluating the  
651 potential of large-scale simulations to predict carbon fluxes of terrestrial ecosystems over  
652 a European Eddy Covariance network, *Biogeosciences Discuss.*, ~~10, 11857-11897~~, [2013,](#)  
653 [11, 2661-2678, 2014](#).
- 654 Beer, C., Reichstein, M., Tomelleri, E., Ciais, P., Jung, M., Carvalhais, N., Rödenbeck, C.,  
655 Arain, M. A., Baldocchi, D., Bonan, G. B., Bondeau, A., Cescatti, A., Lasslop, G.,  
656 Lindroth, A., Lomas, M., Luysaert, S., Margolis, H., Oleson, K. W., Rouspard, O.,  
657 Veenendaal, E., Viovy, N., Williams, C., Woodward, F. I., and Papale, D.: Terrestrial  
658 Gross Carbon Dioxide Uptake: Global Distribution and Covariation with Climate,  
659 *Science*, 329, 834-838, 2010.
- 660 Belshe, E. F., Schuur, E. a. G., and Bolker, B. M.: Tundra ecosystems observed to be CO<sub>2</sub>  
661 sources due to differential amplification of the carbon cycle, *Ecology Letters*, 16, 1307-  
662 1315, 2013.

663 Broquet, G., Chevallier, F., Bréon, F. M., Kadygrov, N., Alemanno, M., Apadula, F., Hammer,  
664 S., Haszpra, L., Meinhardt, F., Morguí, J. A., Necki, J., Piacentino, S., Ramonet, M.,  
665 Schmidt, M., Thompson, R. L., Vermeulen, A. T., Yver, C., and Ciais, P.: Regional  
666 inversion of CO<sub>2</sub> ecosystem fluxes from atmospheric measurements: reliability of the  
667 uncertainty estimates, *Atmos. Chem. Phys.*, 13, 9039-9056, 2013.

668 Canadell, J. G., Ciais, P., Gurney, K., Le Quéré, C., Piao, S., Raupach, M. R., and Sabine, C. L.:  
669 An International Effort to Quantify Regional Carbon Fluxes, *Eos, Transactions American*  
670 *Geophysical Union*, 92, 81-82, 2011.

671 Chatterjee, A., Michalak, A. M., Anderson, J. L., Mueller, K. L., and Yadav, V.: Toward reliable  
672 ensemble Kalman filter estimates of CO<sub>2</sub> fluxes, *Journal of Geophysical Research:*  
673 *Atmospheres*, 117, D22306, 2012.

674 [Globalview-Co2: Cooperative Atmospheric Data Integration Project – Carbon Dioxide \(2010\),](#)  
675 [CD-ROM, NOAA ESRL, Boulder, Colorado, also available at: ftp.cmdl.noaa.gov, Path:](#)  
676 [cgg/co2/GLOBALVIEW\]. NOAA Global Monitoring Division: Boulder, Colorado,](#)  
677 [U.S.A., 2010.](#)

678 Göckede, M., Michalak, A. M., Vickers, D., Turner, D. P., and Law, B. E.: Atmospheric inverse  
679 modeling to constrain regional-scale CO<sub>2</sub> budgets at high spatial and temporal resolution,  
680 *Journal of Geophysical Research: Atmospheres*, 115, D15113, 2010.

681 Gourdji, S. M., Hirsch, A. I., Mueller, K. L., Yadav, V., Andrews, A. E., and Michalak, A. M.:  
682 Regional-scale geostatistical inverse modeling of North American CO<sub>2</sub> fluxes: a  
683 synthetic data study, *Atmos. Chem. Phys.*, 10, 6151-6167, 2010.

684 Gourdji, S. M., Mueller, K. L., Yadav, V., Huntzinger, D. N., Andrews, A. E., Trudeau, M.,  
685 Petron, G., Nehrkorn, T., Eluszkiewicz, J., Henderson, J., Wen, D., Lin, J., Fischer, M.,  
686 Sweeney, C., and Michalak, A. M.: North American CO<sub>2</sub> exchange: inter-comparison of  
687 modeled estimates with results from a fine-scale atmospheric inversion, *Biogeosciences*,  
688 9, 457-475, 2012.

689 Hayes, D. J., Turner, D. P., Stinson, G., Mcguire, A. D., Wei, Y., West, T. O., Heath, L. S., De  
690 Jong, B., Mcconkey, B. G., Birdsey, R. A., Kurz, W. A., Jacobson, A. R., Huntzinger, D.  
691 N., Pan, Y., Post, W. M., and Cook, R. B.: Reconciling estimates of the contemporary  
692 North American carbon balance among terrestrial biosphere models, atmospheric  
693 inversions, and a new approach for estimating net ecosystem exchange from inventory-  
694 based data, *Global Change Biology*, 18, 1282-1299, 2012.

695 Hoeting, J. A., Davis, R. A., Merton, A. A., and Thompson, S. E.: Model Selection For  
696 Geostatistical Models, *Ecological Applications*, 16, 87-98, 2006.

697 Huntzinger, D. N., Gourdji, S. M., Mueller, K. L., and Michalak, A. M.: [A systematic approach](#)  
698 [for comparing modeled biospheric carbon fluxes across regional scales, \*Biogeosciences\*,](#)  
699 [8, 1579-1593, 2011a.](#)

700 ~~Huntzinger, D. N., Gourdji, S. M., Mueller, K. L., and Michalak, A. M.:~~ The utility of  
701 continuous atmospheric measurements for identifying biospheric CO<sub>2</sub> flux variability,  
702 *Journal of Geophysical Research: Atmospheres*, 116, D06110, ~~2011b~~2011.

703 Huntzinger, D. N., Post, W. M., Wei, Y., Michalak, A. M., West, T. O., Jacobson, A. R., Baker,  
704 I. T., Chen, J. M., Davis, K. J., Hayes, D. J., Hoffman, F. M., Jain, A. K., Liu, S.,  
705 Mcguire, A. D., Neilson, R. P., Potter, C., Poulter, B., Price, D., Raczka, B. M., Tian, H.  
706 Q., Thornton, P., Tomelleri, E., Viovy, N., Xiao, J., Yuan, W., Zeng, N., Zhao, M., and  
707 Cook, R.: North American Carbon Program (NACP) regional interim synthesis:  
708 Terrestrial biospheric model intercomparison, *Ecological Modelling*, 232, 144-157, 2012.



709 Keenan, T. F., Baker, I., Barr, A., Ciais, P., Davis, K., Dietze, M., Dragoni, D., Gough, C. M.,  
710 Grant, R., Hollinger, D., Hufkens, K., Poulter, B., Mccaughey, H., Raczka, B., Ryu, Y.,  
711 Schaefer, K., Tian, H., Verbeeck, H., Zhao, M., and Richardson, A. D.: Terrestrial  
712 biosphere model performance for inter-annual variability of land-atmosphere CO<sub>2</sub>  
713 exchange, *Global Change Biology*, 18, 1971-1987, 2012.

714 Kort, E. A., Eluszkiewicz, J., Stephens, B. B., Miller, J. B., Gerbig, C., Nehrkorn, T., Daube, B.  
715 C., Kaplan, J. O., Houweling, S., and Wofsy, S. C.: Emissions of CH<sub>4</sub> and N<sub>2</sub>O over the  
716 United States and Canada based on a receptor-oriented modeling framework and  
717 COBRA-NA atmospheric observations, *Geophysical Research Letters*, 35, L18808, 2008.

718 Krinner, G., Viovy, N., De Noblet-Ducoudré, N., Ogée, J., Polcher, J., Friedlingstein, P., Ciais,  
719 P., Sitch, S., and Prentice, I. C.: A dynamic global vegetation model for studies of the  
720 coupled atmosphere-biosphere system, *Global Biogeochemical Cycles*, 19, GB1015,  
721 2005.

722 Lin, J. C., Gerbig, C., Wofsy, S. C., Andrews, A. E., Daube, B. C., Davis, K. J., and Grainger, C.  
723 A.: A near-field tool for simulating the upstream influence of atmospheric observations:  
724 The Stochastic Time-Inverted Lagrangian Transport (STILT) model, *Journal of*  
725 *Geophysical Research: Atmospheres*, 108, 4493, 2003.

726 Mcguire, A. D., Christensen, T. R., Hayes, D., Heroult, A., Euskirchen, E., Kimball, J. S.,  
727 Koven, C., Lafleur, P., Miller, P. A., Oechel, W., Peylin, P., Williams, M., and Yi, Y.: An  
728 assessment of the carbon balance of Arctic tundra: comparisons among observations,  
729 process models, and atmospheric inversions, *Biogeosciences*, 9, 3185-3204, 2012.

730 Mckain, K., Wofsy, S. C., Nehrkorn, T., Eluszkiewicz, J., Ehleringer, J. R., and Stephens, B. B.:  
731 Assessment of ground-based atmospheric observations for verification of greenhouse gas  
732 emissions from an urban region, *Proceedings of the National Academy of Sciences*, 109,  
733 8423-8428, 2012.

734 [Michalak, A. M., Bruhwiler, L., and Tans, P. P.: A geostatistical approach to surface flux](#)  
735 [estimation of atmospheric trace gases, \*Journal of Geophysical Research: Atmospheres\*,](#)  
736 [109, D14109, 2004.](#)

737 Miles, N. L., Richardson, S. J., Davis, K. J., Lauvaux, T., Andrews, A. E., West, T. O., Bandaru,  
738 V., and Crosson, E. R.: Large amplitude spatial and temporal gradients in atmospheric  
739 boundary layer CO<sub>2</sub> mole fractions detected with a tower-based network in the U.S. upper  
740 Midwest, *Journal of Geophysical Research: Biogeosciences*, 117, G01019, 2012.

741 Mueller, K. L., Yadav, V., Curtis, P. S., Vogel, C., and Michalak, A. M.: Attributing the  
742 variability of eddy-covariance CO<sub>2</sub> flux measurements across temporal scales using  
743 geostatistical regression for a mixed northern hardwood forest, *Global Biogeochemical*  
744 *Cycles*, 24, 2010.

745 Ogle, S., Davis, K., Andrews, A., West, T., Cook, R., Parkin, R., Morisette, J., Verma, S., and  
746 Wofsy, S.: Science Plan: Mid-Continent Intensive Campaign. Greenbelt, Md., 2006.

747 [Peters, W., Jacobson, A. R., Sweeney, C., Andrews, A. E., Conway, T. J., Masarie, K., Miller, J.](#)  
748 [B., Bruhwiler, L. M. P., Pétron, G., Hirsch, A. I., Worthy, D. E. J., Van Der Werf, G. R.,](#)  
749 [Randerson, J. T., Wennberg, P. O., Krol, M. C., and Tans, P. P.: An atmospheric](#)  
750 [perspective on North American carbon dioxide exchange: CarbonTracker, \*Proceedings of\*](#)  
751 [the National Academy of Sciences, 104, 18925-18930, 2007.](#)

752 [Pillai, D., Gerbig, C., Kretschmer, R., Beck, V., Karstens, U., Neininger, B., and Heimann, M.:](#)  
753 [Comparing Lagrangian and Eulerian models for CO<sub>2</sub> transport – a step towards Bayesian](#)  
754 [inverse modeling using WRF/STILT-VPRM, \*Atmos. Chem. Phys.\*, 12, 8979-8991, 2012.](#)

755 Ping, C.-L., Michaelson, G. J., Jorgenson, M. T., Kimble, J. M., Epstein, H., Romanovsky, V. E.,  
756 and Walker, D. A.: High stocks of soil organic carbon in the North American Arctic  
757 region, *Nature Geosci*, 1, 615-619, 2008.

758 Raczka, B. M., Davis, K. J., Huntzinger, D. N., Neilson, R., Poulter, B., Richardson, A., Xiao, J.,  
759 Baker, I., Ciais, P., Keenan, T. F., Law, B., Post, W. M., Ricciuto, D., Schaefer, K., Tian,  
760 H., Tomelleri, E., Verbeeck, H., and Viovy, N.: Evaluation of continental carbon cycle  
761 simulations with North American flux tower observations, *Ecological Monographs*, 83,  
762 531-556, 2013.

763 Richardson, A. D., Anderson, R. S., Arain, M. A., Barr, A. G., Bohrer, G., Chen, G., Chen, J. M.,  
764 Ciais, P., Davis, K. J., Desai, A. R., Dietze, M. C., Dragoni, D., Garrity, S. R., Gough, C.  
765 M., Grant, R., Hollinger, D. Y., Margolis, H. A., Mccaughey, H., Migliavacca, M.,  
766 Monson, R. K., Munger, J. W., Poulter, B., Raczka, B. M., Ricciuto, D. M., Sahoo, A. K.,  
767 Schaefer, K., Tian, H., Vargas, R., Verbeeck, H., Xiao, J., and Xue, Y.: Terrestrial  
768 biosphere models need better representation of vegetation phenology: results from the  
769 North American Carbon Program Site Synthesis, *Global Change Biology*, 18, 566-584,  
770 2012.

771 Sasai, T., Ichii, K., Yamaguchi, Y., and Nemani, R.: Simulating terrestrial carbon fluxes using  
772 the new biosphere model “biosphere model integrating eco-physiological and  
773 mechanistic approaches using satellite data” (BEAMS), *Journal of Geophysical Research:*  
774 *Biogeosciences*, 110, G02014, 2005.

775 Schaefer, K., Schwalm, C. R., Williams, C., Arain, M. A., Barr, A., Chen, J. M., Davis, K. J.,  
776 Dimitrov, D., Hilton, T. W., Hollinger, D. Y., Humphreys, E., Poulter, B., Raczka, B. M.,  
777 Richardson, A. D., Sahoo, A., Thornton, P., Vargas, R., Verbeeck, H., Anderson, R.,  
778 Baker, I., Black, T. A., Bolstad, P., Chen, J., Curtis, P. S., Desai, A. R., Dietze, M.,  
779 Dragoni, D., Gough, C., Grant, R. F., Gu, L., Jain, A., Kucharik, C., Law, B., Liu, S.,  
780 Lokipitiya, E., Margolis, H. A., Matamala, R., Mccaughey, J. H., Monson, R., Munger, J.  
781 W., Oechel, W., Peng, C., Price, D. T., Ricciuto, D., Riley, W. J., Roulet, N., Tian, H.,  
782 Tonitto, C., Torn, M., Weng, E., and Zhou, X.: A model-data comparison of gross  
783 primary productivity: Results from the North American Carbon Program site synthesis,  
784 *Journal of Geophysical Research: Biogeosciences*, 117, G03010, 2012.

785 Schuur, E. a. G., Vogel, J. G., Crummer, K. G., Lee, H., Sickman, J. O., and Osterkamp, T. E.:  
786 The effect of permafrost thaw on old carbon release and net carbon exchange from  
787 tundra, *Nature*, 459, 556-559, 2009.

788 Schwalm, C. R., Williams, C. A., Schaefer, K., Anderson, R., Arain, M. A., Baker, I., Barr, A.,  
789 Black, T. A., Chen, G., Chen, J. M., Ciais, P., Davis, K. J., Desai, A., Dietze, M.,  
790 Dragoni, D., Fischer, M. L., Flanagan, L. B., Grant, R., Gu, L., Hollinger, D., Izaurrealde,  
791 R. C., Kucharik, C., Lafleur, P., Law, B. E., Li, L., Li, Z., Liu, S., Lokupitiya, E., Luo,  
792 Y., Ma, S., Margolis, H., Matamala, R., Mccaughey, H., Monson, R. K., Oechel, W. C.,  
793 Peng, C., Poulter, B., Price, D. T., Ricciuto, D. M., Riley, W., Sahoo, A. K., Sprintsin, M.,  
794 Sun, J., Tian, H., Tonitto, C., Verbeeck, H., and Verma, S. B.: A model-data  
795 intercomparison of CO<sub>2</sub> exchange across North America: Results from the North  
796 American Carbon Program site synthesis, *Journal of Geophysical Research:*  
797 *Biogeosciences*, 115, 566-584, 2010.

798 Shiga, ~~Y. P., Y., Anna, M., Michalak, A.~~ M., Gourdji, S. M., Mueller, K. L., and Yadav, V.:  
799 Detecting fossil fuel emissions patterns from ~~sub-continental~~subcontinental regions using

800 | North American in-situ CO2 measurements ~~Geophys. Res. Lett., Submitted, Geophysical~~  
801 | ~~Research Letters, 41, 2014GL059684, 2014.~~  
802 | Skamarock, W. C. and Klemp, J. B.: A time-split nonhydrostatic atmospheric model for weather  
803 | research and forecasting applications, *J. Comput. Phys.*, 227, 3465-3485, 2008.  
804 | Tarnocai, C., Canadell, J. G., Schuur, E. a. G., Kuhry, P., Mazhitova, G., and Zimov, S.: Soil  
805 | organic carbon pools in the northern circumpolar permafrost region, *Global*  
806 | *Biogeochemical Cycles*, 23, GB2023, 2009.  
807 | Turner, D. P., Göckede, M., Law, B. E., Ritts, W. D., Cohen, W. B., Yang, Z., Hudiburg, T.,  
808 | Kennedy, R., and Duane, M.: Multiple constraint analysis of regional land-surface  
809 | carbon flux, *Tellus B*, 63, 207-221, 2011.  
810 | Van Der Werf, G. R., Randerson, J. T., Giglio, L., Collatz, G. J., Kasibhatla, P. S., and Arellano  
811 | Jr, A. F.: Interannual variability in global biomass burning emissions from 1997 to 2004,  
812 | *Atmos. Chem. Phys.*, 6, 3423-3441, 2006.  
813 | Yadav, V., Mueller, K. L., Dragoni, D., and Michalak, A. M.: A geostatistical synthesis study of  
814 | factors affecting gross primary productivity in various ecosystems of North America,  
815 | *Biogeosciences*, 7, 2655-2671, 2010.  
816 | Yadav, V., Mueller, K. L., and Michalak, A. M.: A backward elimination discrete optimization  
817 | algorithm for model selection in spatio-temporal regression models, *Environmental*  
818 | *Modelling & Software*, 42, 88-98, 2013.  
819 | Zeng, N., Mariotti, A., and Wetzel, P.: Terrestrial mechanisms of interannual CO2 variability,  
820 | *Global Biogeochemical Cycles*, 19, GB1016, 2005.  
821 |  
822 |

823 **Figures**

824 Figure 1. North American biomes, modified from Olson (2001), as defined for the case studies;  
825 stars green triangles indicate the locations of atmospheric CO<sub>2</sub> measurement towers used in the  
826 analysis.

827 Figure 2. Illustration of the 1°×1° and 3-hourly spatiotemporal variability of NEE simulated by  
828 CASA-GFED for Boreal Forests and Taiga in July. A vector including these 1°×1° and 3-hourly  
829 fluxes corresponds to one ancillary variable (i.e. one column) in  $X$

830 Figure 3. Illustration of Synthetic Data (SD) case studies as described in Section 4.

831 Figure 34. Average numbers of months within each season for which the candidate TBM is  
832 selected for the SD-one- $\emptyset\emptyset$ , SD-one- $\emptyset\epsilon$  and SD-one- $\xi\epsilon$  case studies (Figure 23). Grey shading  
833 in SD-one- $\xi\epsilon$  represents biomes that were determined not to be well constrained by available  
834 atmospheric data. DJF: December, January, February; MAM: March, April, May; JJA: June,  
835 July, August; SON: September, October, November. The criteria for grey areas includes: 1) no  
836 models are selected in one season; or 2) the overall model selection is less than 50% in a year.

837 Figure 45. Average numbers of months within each season for which the candidate TBM is  
838 selected for the SD-all- $\xi\epsilon$  case study (Figure 23). Grey shading represents biomes that were  
839 determined not to be well constrained by available atmospheric data. DJF: December, January,  
840 February; MAM: March, April, May; JJA: June, July, August; SON: September, October,  
841 November.

842 Figure 56. The correlation coefficient of NEE spatiotemporal series as simulated by different  
843 TBMs throughout 2008 for the four biomes better constrained by available atmospheric  
844 observations. TGSS: Temperate Grasslands, Savannas, Shrublands; Bore: Boreal Forests and  
845 Taiga; TCoF: Temperate Coniferous Forests; TBMF: Temperate Broadleaf and Mixed Forests.

846 Figure 67. Number of TBMs that are selected for each biome-month in the RD-one- $\xi\epsilon$  cases  
847 study. Grey shading represents biomes that were determined not to be well constrained by  
848 available atmospheric data.

849 Figure 78. The TBM that explains the most variability in atmospheric measurements for a given  
850 biome-month, as identified by the RD-all- $\xi\epsilon$  experiment. Grey shading represents biomes that  
851 were determined not to be well constrained by available atmospheric data.

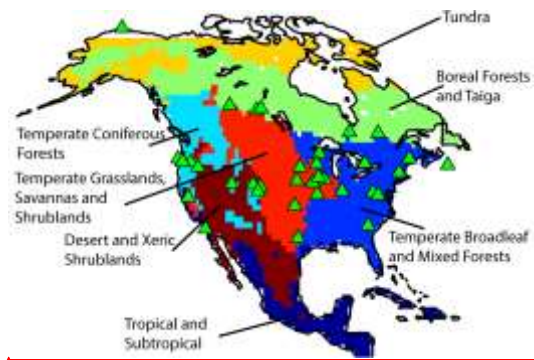
852

853

Figures

854

Figure 1

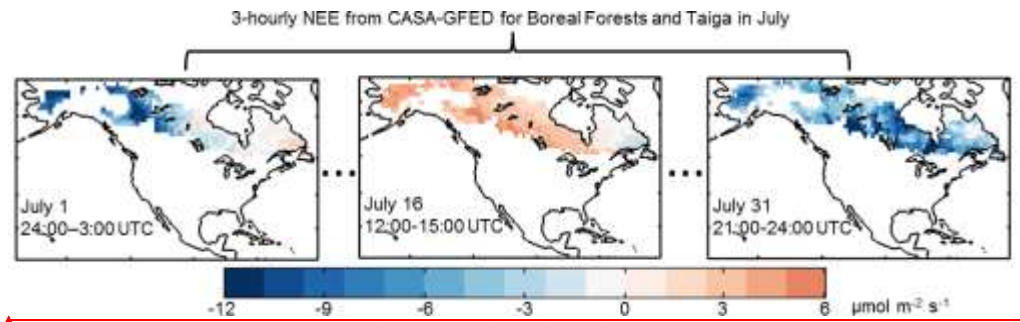


Formatted: Font: 12 pt

855

856

Figure 2

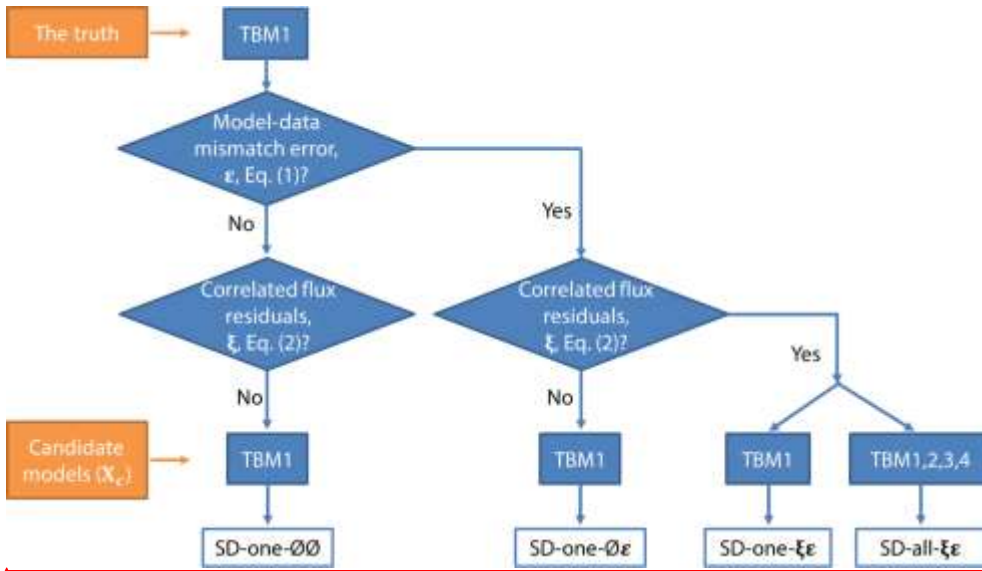


Formatted: Font: 12 pt

857

858

Figure 3

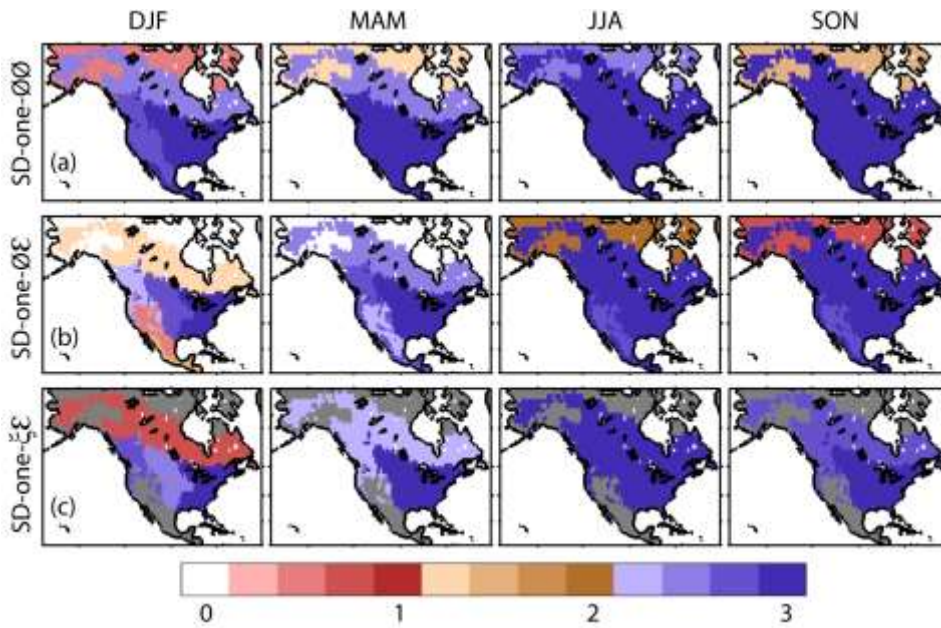


Formatted: Font: 12 pt

859

860

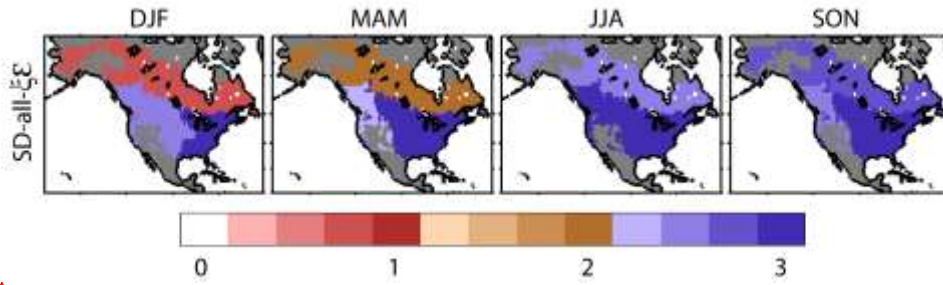
Figure 4



Formatted: Font: 12 pt

861

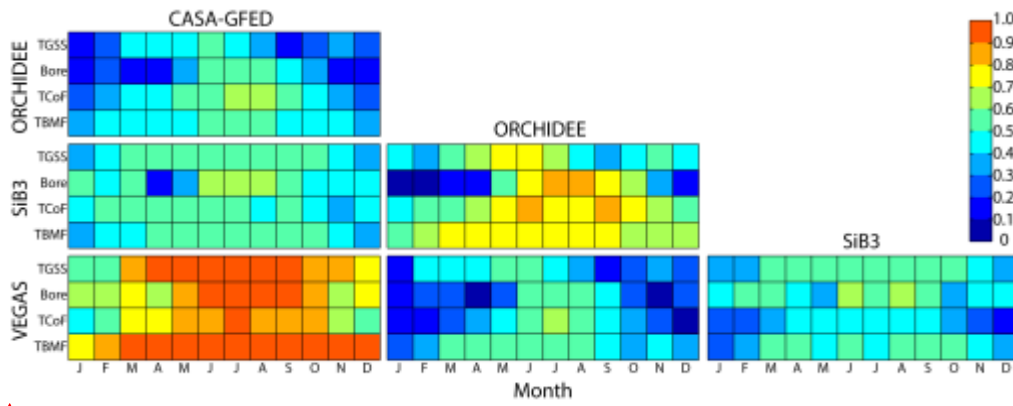
862 [Figure 5](#)



Formatted: Font: 12 pt

863

864 [Figure 6](#)

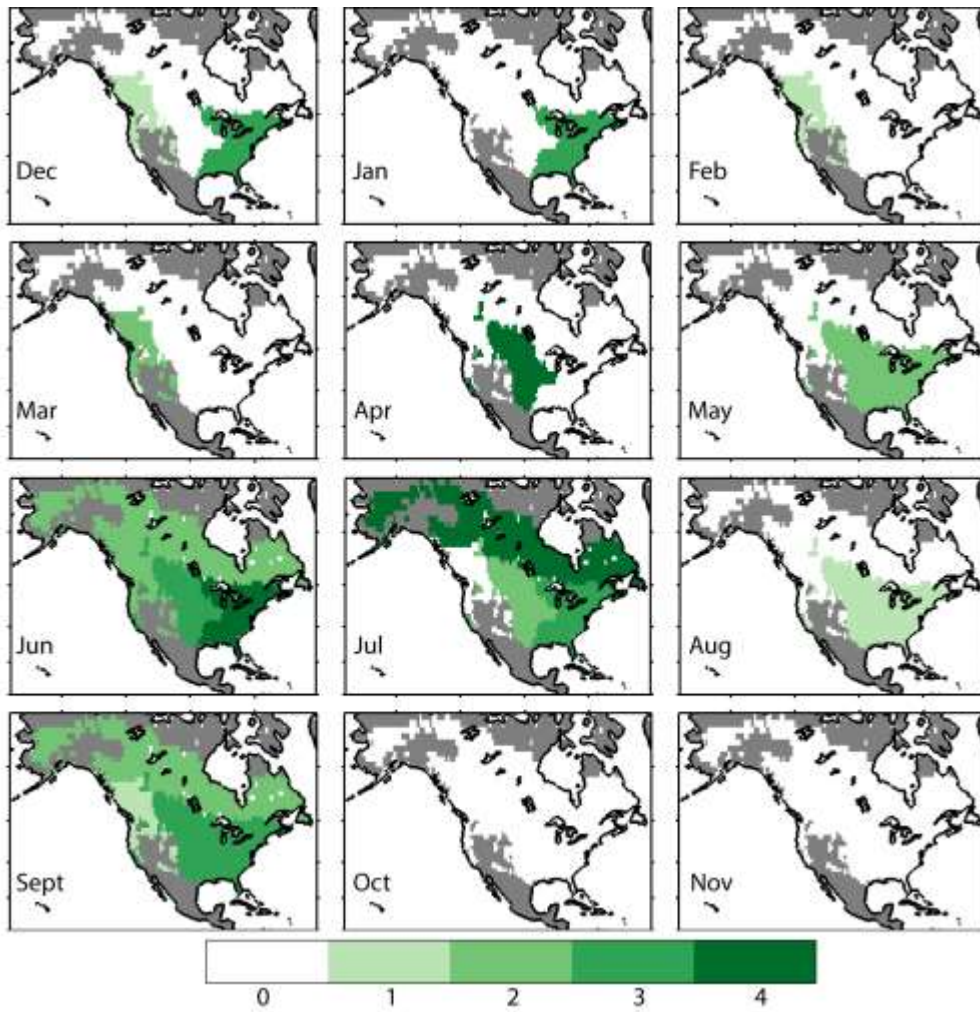


Formatted: Font: 12 pt

865

866

Figure 7



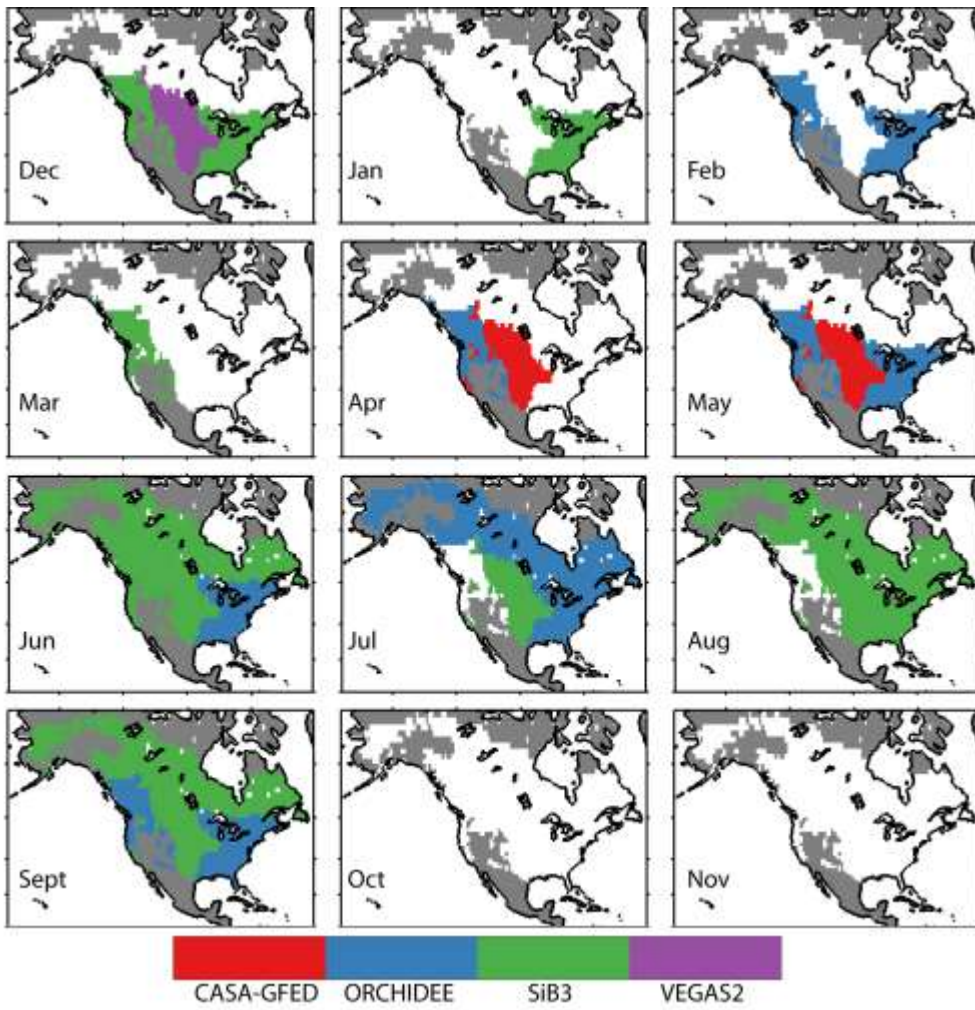
867

Formatted: Font: 12 pt



868

Figure 8



869

870

Formatted: Font: 12 pt